Magnetic reversal of ultra-thin films with planar magnetization

R.A. Hyman[1*], A. Zangwill[1], and M.D. Stiles[2]

[1]*School of Physics, Georgia Institute of Technology, Atlanta, GA 30332-0430*

[2]*Electron Physics Group, National Institute of Standards and Technology, Gaithersburg, MD 20899*

(December 2, 1999)

Abstract

Classical spin simulations are used to study magnetic reversal in ultra-thin (1-6 monolayers) films with planar magnetization and surface roughness typical of epitaxially grown samples. Reduced site symmetry at surface steps leads to strong, local anisotropies that both nucleate reversal and pin domain wall motion. The results we obtain from realistic models with periodic roughness are interpreted using a much simpler model with a single, finite-length step. These models show how growth induced roughness can lead to oscillations in the coercive field as the film thickness is increased, as seen in some experiments. They also demonstrate explicitly how local step anisotropies become less important and magnetostatic interactions become more important as the film thickness increases.

PACS numbers: 75.70.-i,75.60.-d

I. INTRODUCTION

The potential for novel physics and exciting applications has motivated many studies of ultra-thin magnetic films [1]. To explore new physics, it is usual to focus on simple model systems and equilibrium properties such as exchange, anisotropy, and the thermodynamic phase diagram in the space of temperature and thickness. To exploit new applications, it is typical to study more complex systems and non-equilibrium properties such as hysteresis, domain wall motion, and magneto-transport. Common to both is the observation that variations in surface roughness and film morphology often have a significant effect on magnetic structure.

Magnetometry [2] and the surface magneto-optic Kerr effect [3] are widely used to probe magnetization reversal in ultra-thin films. A typical experiment reports representative hysteresis loops and the coercive field as a function of total deposited material. It is generally appreciated that the films in question exhibit surface roughness, but the consequences of this fact are not often addressed explicitly. One exception is a theoretical argument presented a few years ago by Bruno [4]. Making simple assumptions regarding thickness fluctuations and the nature of domain wall pinning in films with *perpendicular magnetization*, he derived a coercive field $H_C \propto t^{-5/2}$ where t is the film thickness. Experimental tests of this prediction for the Co/Pd(111) [5] agree and Co/Pt(111) [6] systems are not consistent with each other.

Our interest here is hysteresis and coercivity in ultra-thin films with *planar magnetization*. Roughness is very important in such systems because surface steps break translational invariance and thereby induce local, in-plane anisotropies that differ from the intrinsic in-plane anisotropy of the flat film [7,8]. This is significant because, as stressed by Arrott [9], local anisotropies can nucleate and pin domain walls during the magnetization process. The corresponding hysteresis can be very complex indeed [10].

The phenomenon considered by Bruno–the variation of domain wall energy with local film thickness–is present for planar magnetized films as well. Indeed, Kolesik *et al.* have studied its effect on the magnetic reversal of an Fe/W(110) sesquilayer film using a planar

Ising simulation [11]. They did not investigate the effect of step-induced anisotropy. In this work, we take account of both effects.

Our work was motivated by experiments such as those published recently for the ultra-thin Co/Cu(001) system. The measured coercivity shows sub-monolayer oscillations superimposed on a monotonic increase with thickness for 2-15 monolayers of deposited cobalt [12]. Similarly, the coercivity of Cu/Co/Cu(001) is strongly non-monotonic for 0-2 monolayers of deposited copper [13].

We use a simple but realistic simulation model of magnetic reversal to show how typical epitaxial growth surface morphologies can lead to oscillatory and other non-monotonic behaviors for the coercive field of planar magnetized ultra-thin films. This work extends to the multilayer regime previous theoretical and simulation work by the authors for the case of monolayer-height islands on a single complete layer [14,15]. It also exploits a new conceptual framework developed by the authors to understand magnetization reversal in *vicinal* samples [16].

We are interested in film morphologies typical of ultra-thin magnets grown epitaxially on a non-magnetic substrate. In the cartoon version of such a film shown in Fig. 1(a), several completed magnetic layers lie beneath multilevel roughness in the form of irregular pits and islands. Needless to say, some simplification is required in order to perform a trend study as we wish to do.

Figure 1(c) and Figure 1(d) show the morphologies we have chosen to study in detail. They consist of several completed magnetic layers with *one* incomplete layer in the form of a regular array of square islands or pits. These two limiting cases turn out to be sufficient to capture most of the physics of the more realistic morphology. In fact, the essential roles of step length and step anisotropy in magnetic reversal are captured already by the even simpler "isolated step" model shown in Fig. 1(b). The islands and pits add the effects of step separation and magnetostatics.

The plan of our paper is as follows. Section II focuses on the isolated step model. We catalog the various hysteresis loop topologies that occur and correlate them with the

dimensionless control parameters of the model in the form of a phase diagram. Section III is a discussion of the island model including the effect of magnetostatics. Results are presented for the hysteresis loops and the coverage dependence of the coercive field. The isolated step model is used to rationalize the global behavior. Section IV briefly discusses the pit model, a synthetic island + pit model, and compares our results with experiment. Section V is a summary.

II. THE ISOLATED STEP MODEL

The model film of Fig. 1(b) is one monolayer thick and lies on a flat non-magnetic substrate. Every atomic site in the film carries a spin that is constrained to lie in the plane of the surface. Ferromagnetic exchange J couples nearest neighbor spins and a four-fold planar anisotropy K_4 acts on every spin. The effect of an isolated step is modeled by adding an additional two-fold planar anisotropy K_2 along a line segment of width W. Thicker films can be modeled by varying the exchange and anisotropy constants because we assume that the magnetization does not vary in the direction perpendicular to the film surface. The direction of the two-fold axis is perpendicular to the step and parallel to one of the four-fold axes. An external magnetic field H is applied parallel to the step. Magnetostatics is ignored.

The hysteresis curves for this model were found from numerical simulations of a classical spin Hamiltonian (see below) that incorporates all the features outlined above. We find only "one-jump" and "two-jump" hysteresis loops over the entire range of parameters. Subtle differences divide each of these into three sub-classes. The six typical loops that occur (Fig. 2) are characterized by the fields H_N, H_S, and H_T where characteristic changes in the magnetization occur [17]. In the discussion to follow, we consider external fields increasing from large negative values to large positive values. The characteristic fields H_S, and H_T are always positive, but H_N can have either sign. The rationale for the Roman numeral loop labels will be explained below.

We focus first on loop III(a) because every feature of the reversal mechanism is reflected

separately in its structure. The first deviation of the magnetization from saturation occurs at the "nucleation field" H_N. Spins within a few exchange lengths of the step rotate coherently away from the saturation direction (180°) because of the torque exerted by K_2. At the end of this interval of smoothly changing magnetization, a lens-shaped domain has formed with approximately-90° domain walls interposed between the step spins and the terrace spins [14]. At the "step instability field" H_S, the domain walls depin from the step and sweep across the film. This leaves the system in a "90° state" with nearly zero magnetization along the direction of H. Another regime of coherent rotation follows until H_T when a Stoner-Wohlfarth [18] type instability occurs on the terrace far from the step. When this happens, the terrace spins coherently jump from the 90° state to the 0° reversed state. The step spins lag slightly behind because they feel the pinning effect of K_2. Smooth coherent rotation completes the reversal process.

The IV loops generically have one jump because the terrace instability formally occurs *before* the step instability (domain wall depinning) in these cases. Of course, the spins cannot jump coherently from 90° to 0° until they get to 90° in the first place. As a result, the spins rotate all the way to near reversal as soon the domain walls depin from the step.

The difference between loops III(a) and III(b) and between loops IV(a) and IV(b) depends on whether or not K_2 is large enough to prevent the terrace jump from "dragging" the step spins all the way to saturation at H_T. The loops III(c) and IV(c) differ from their (b) counterparts because the step instability formally occurs before nucleation. When this is the case, the domain walls depin from the step as soon as nucleation occurs.

Figure 3 is a phase diagram derived from our simulations that connects the loop topologies ("the phases") to the model parameters. As the diagram axes show, the latter are best organized into the dimensionless parameters $\mathcal{K} = K_2/2\sigma$ and $\mathcal{W} = W/\delta$. The first of these is the step anisotropy scaled by the domain wall energy $\sigma = \sqrt{2JK_4}$. The second is the step width scaled by the exchange length $\delta = \sqrt{J/2K_4}$. The particular numerical range of $\mathcal{K}$ and $\mathcal{W}$ used in Fig. 3 arises when realistic values are chosen for the physical parameters (see below).

The phases have been labeled for consistency with our previous vicinal surface results [16] where the characteristic fields H_N, H_S, and H_T occur also [19]. Indeed, the phase diagram here and the one derived in Ref. [16] are simply two-dimensional slices of a three-dimensional phase diagram with axes: scaled step anisotropy $\mathcal{K}$, scaled step width $\mathcal{W}$ and scaled terrace length $\mathcal{L}$. The phase diagram for the vicinal film is the two-dimensional slice at $\mathcal{W} \to \infty$. The phase diagram for the single step limit is the perpendicular slice at $\mathcal{L} \to \infty$. There is a phase boundary between these two slices at $\mathcal{L} \to \infty$ and $\mathcal{W} \to \infty$ (where $H_S = 0$) that separates phases IIa and IIb in the vicinal film from phases IIIa and IIIb in the finite step film.

The general placement of the various phases in Fig. 3 can be understood from the variation of the characteristic fields with $\mathcal{W}$ and $\mathcal{K}$. These are shown in Fig. 4 and Fig. 5, respectively, scaled by the Stoner-Wohlfarth field $H_{SW} = 8a^2K_4/\mu$. The latter is the external field value at which easy-axis reversal occurs for a single domain system with four-fold anisotropy [18]. From Fig. 3, we see that the III phases appear at larger values of $\mathcal{W}$ than the IV phases. $H_T = \sqrt{6}/9 H_{SW}$ [16] is independent of step width (it is driven by the terrace spins) while H_S smoothly decreases with $\mathcal{W}$. This guarantees that the curves of H_S and H_T in Fig. 4 eventually cross as $\mathcal{W}$ increases and the III phases supplant the IV phases. The field H_S decreases with $\mathcal{W}$ for the following reason [15]. As H increases, the lens domain expands to gain Zeeman energy. This is opposed by the domain wall energy which is proportional to the domain perimeter. The domain wall depins when these two balance. One gets $H_S \propto 1/\mathcal{W}$ because the domain wall is pinned at opposite ends of the step.

The (a)→(b) and (b)→(c) transitions in Fig. 3 occur with decreasing $\mathcal{K}$. The first of these agrees with the "dragging" argument given above. That is, when the step anisotropy is large, the Stoner-Wohlfarth instability of the terrace spins does not produce enough torque to rotate the step spins to complete reversal. But when $\mathcal{K}$ is small enough, a direct jump to 0° is possible. The (b)→(c) transition occurs because H_N increases (in magnitude) past H_S as the step anisotropy is reduced. This happens because, as noted earlier, easy (small magnitude) nucleation is encouraged by the torque exerted by K_2 on the step spins.

These results are sufficient to qualitatively explain the experimental observation noted earlier [12] that the coercive field H_C rises rapidly with deposited material with a small amplitude oscillation superimposed. We need only recall that $\mathcal{K} = K_2/2\sigma$ where $\sigma = \sqrt{2JK_4}$ is the domain wall energy. The latter is proportional to the film thickness so $\mathcal{K} \propto t^{-1}$. Figure 5 then shows that H_C should indeed increase rapidly at t increases, at least for larger thicknesses. On the other hand, it is well understood that the step density oscillates as growth proceeds [20]. This translates into oscillations in $\mathcal{W}$ in the present model so Fig. 4 implies that oscillations will occur in the coercive field as well. When $H_C = H_N$ (small $\mathcal{K}$), the oscillation amplitude is smaller or comparable to the overall change in H_C. When $H_C = H_S$ (large $\mathcal{K}$), the oscillation amplitude is comparable or larger than the change in the coercive field.

III. THE ISLAND MODEL

The periodic surface morphologies shown in Fig. 1 permit us to model the variations in step length and step separation that occur during growth in a fairly realistic manner. In both cases, the square structures have center-to-center separation D and side length L. If the flat surface has t complete magnetic layers, Fig. 1(c) and Fig. l(d) will be called the island and pit models, respectively. In this section, we focus on the island model exclusively.

Except for the addition of magnetostatics, the magnetic energy we used to study hysteresis in the island model is the same as the one we used to analyze the isolated step model. In detail, the substrate is taken as centered cubic so the thickness t is measured in units of $t_0 = a/2$ where a is the in-plane lattice constant. Classical Heisenberg spins at each surface site i point in the direction $\hat{\mathbf{S}}_i$. We get a two-dimensional model because the spins are forced to be parallel within each atomic column. This is acceptable because we limit ourselves to values of t that are much less than the exchange length.

Each spin is subject to nearest-neighbor ferromagnetic exchange J, a large two-fold perpendicular surface anisotropy $K_Z > 0$, a four-fold planar anisotropy $K_4 > 0$, an external

field $\mathbf{H}$, and magnetic dipole-dipole interactions from all other spins. The saturation magnetization is M_S and a two-fold anisotropy K_2 is present at step edge sites only. The magnetic energy is

$$\begin{aligned} E_M = &- \sum_{\langle i,j \rangle} J_{ij} \hat{\mathbf{S}}_i \cdot \hat{\mathbf{S}}_j - a^2 K_2 \sum_{i \in step} (\hat{\mathbf{S}}_i \cdot \hat{\mathbf{b}}_i)^2 \\ &-2a^2 K_4 \sum_i t_i \left[(\hat{S}_i^x)^4 + (\hat{S}_i^y)^4 \right] - \mu \mathbf{H} \cdot \sum_i t_i \hat{\mathbf{S}}_i \\ &+a^2 K_Z \sum_i (\hat{S}_i^z)^2 - \frac{\mu}{2} \sum_i t_i \hat{\mathbf{S}}_i \cdot \mathbf{H}_{INT} \end{aligned} \tag{1}$$

where t_i is the film height at site i in units of t_0, $\hat{\mathbf{b}}_i$ is a unit vector parallel to the local step edge, $J_{ij} = J \min[t_i, t_j]$, and $\mu = \mu_0 a^2 t_0 M_S$ where μ_0 is the magnetic constant (a k a permeability of free space) in SI units.

The internal magnetostatic field $\mathbf{H}_{INT}$ was calculated by solving the discretized Maxwell equations $\nabla \cdot \mathbf{H}_{INT} = -\nabla \cdot \mathbf{M}$ and $\nabla \times \mathbf{H}_{INT} = 0$. For this calculation an effective surface layer with uniform thickness was used to exploit a two-dimensional fast Fourier transform algorithm designed for a thin film with no surface roughness [21].

Typical values of the material parameters, $J = 10^{-21}$ J and $K_4 = 1 \times 10^{-3}$ mJ/m^2, [22] imply, in the absence of magnetostatics, a domain wall energy per unit length $\sigma = t\sqrt{2JK_4} \approx t \times 10^{-14}$ J/m and an exchange length $\delta = \sqrt{J/2K_4} \approx 20$ nm. The numerical results reported below all use the values $|K_2| = K_Z = 1$ mJ/m^2 [2], $a = 0.3$ nm, and $M_S = 1.44 \times 10^6$ A/m (1440 emu/cm^3), in addition to those quoted above for J and K_4. The lengths L and D are measured in spin block units of $10a \approx \delta/7$, a distance over which no appreciable spin rotation occurs. Positive step anisotropy $K_2 > 0$ corresponds to a preferred spin axis parallel to the step edges while negative step anisotropy $K_2 < 0$ corresponds to a preferred spin axis perpendicular to the step edges.

The simulation technique was the same as described previously [14]. Beginning with a large value of $\mathbf{H} = H\hat{x} \parallel [100]$, the local minimum of Eq. (1) was followed as the field was reversed adiabatically by a combination of conjugate gradient minimization and relaxational spin dynamics. The magnetization parallel to $\mathbf{H}$ was computed directly from the

corresponding spin configurations.

Figure 6 illustrates the variation of the computed coercive field H_C with total coverage $\Theta = t + \theta$ (in monolayers) for the island model. The islands contribute the partial coverage $\theta = (L/D)^2$ to the total. To mimic a typical growth scenario, the island separation was fixed at $D = 64$ and the coverage was increased by increasing the island dimension L. The heavy (light) dashed curves are for step anisotropies that favors spin alignment parallel (perpendicular) to the step. The solid curve was computed without magnetostatics. There is only one such curve because the magnetic energy Eq. (1) is invariant if $K_2 \to -K_2$ and we rotate the Cartesian axes (from which the spin angles are measured) by 90° in the plane.

For simplicity, we discuss the case of no magnetostatics first. The most striking features in Fig. 6 are the periodic maxima where $H_C = H_{SW}$. These are actually *artifacts* of the growth scenario sketched above because they correspond to perfect layer completion and perfect Stoner-Wohlfarth reversal at integer values of thickness. We will correct for this artifact qualitatively in the next section. Another major trend in Fig. 6 is that H_C decreases very rapidly as each layer begins to grow [14]. This may be understood immediately from the lower panel of Fig. 4 for the isolated step model where H_C is given by either H_N or H_S. Both decrease rapidly, especially when $\mathcal{W}$, *i.e.*, θ is small. Notice that our parameter choices for the island model are such that the full range of $\mathcal{W}$ in this figure corresponds to about $\theta \sim 1/5$.

Another trend seen in Fig. 6 is that the coercive field averaged over each partial monolayer apparently decreases slowly until about $\Theta = 3$ and then increases rapidly. In fact, the behavior of H_C as t increases by integer amounts for *fixed* values of the partial coverage θ depends very strongly on θ. Figure 7 and Figure 8 illustrate this for $\theta = 0.06$ and $\theta = 0.76$, respectively. The $\theta = 0.06$ curves shown in Fig. 7 are directly interpretable using the isolated step model. The sequence shown illustrates the transition from phase IV(b) to phase IV(c) loops. The coercive field is set by H_N and its increase (in magnitude) as t increases (so $\mathcal{K}$ decreases) is clear from Fig. 5. In this regime, the coercive field is a monotonic function of t.

Technically, neither the upper panel ($t = 1$) nor middle panel ($t = 3$) of Fig. 8 belong to the phase diagram of Fig. 3 because both have additional magnetization jumps associated with the presence of multiple steps. The associated changes in the magnetization affects the coercive field [$H_C = H_T$ for these two cases; this never occurs for the single step model] much more than they affect the characteristic fields H_N, H_S, and H_T. Moreover, the values of $\mathcal{K}$ used in Fig. 4 are nearly the same as the ones for the cases under discussion. Notice that the step instabilities in Fig. 8 (H_S for $t = 1$ and H_N for $t = 3$) occur at practically the same value of external field as they do in Fig. 4. H_C is larger at $t = 1$ than $t = 3$ because the step edges *parallel* to the field inhibit the coherent rotation of terrace spins to the 90° state more effectively when $\mathcal{K}$ is larger. This effect is absent from the isolated step model. By the time we reach $t = 5$ (lower panel of Fig. 8), $\mathcal{K}$ is so small that H_N determines the coercivity in phase IV(c) at the large value implied by Fig. 4. Evidently, H_C is not always a monotonic function of film thickness.

Finally, we remark on the very rapid decrease in the coercive field that occurs near layer completion ($\theta \simeq 1$) when Θ is large in Fig. 6. In this regime, $H_C = H_N$ as we have discussed and the film consists of large islands that are closely spaced. Nucleation occurs very readily in this circumstance both because the steps are long and because they are close together. The long length simply generates more torque. The step proximity effectively doubles $\mathcal{K}$ (if the step separation is less than an exchange length [16]) and therefore enhances nucleation as well. Of course, this effect is also absent from the single step model.

We turn now to the influence of magnetostatics reflected in Figure 6. This contribution to the energy is extensive and so has little effect until the film begins to thicken. Dipole interactions then generally increase H_C although the effect is far more pronounced when the step anisotropy is perpendicular to the steps than when it is parallel to the steps. Because $H_C = H_N$ in the relevant regime, we can understand this by rewriting the magnetic energy in the form

$$E_{D-D} = \frac{\mu_0}{2} \int d^3r \int d^3r' \frac{\nabla \cdot M(r) \nabla \cdot M(r')}{|r - r'|}. \tag{2}$$

This term clearly disfavors the creation of "magnetic charge" with density $\nabla \cdot M(r)$. This has two consequences, both of which break the symmetry between parallel and perpendicular anisotropy. First, the magnetization is larger on the islands than on the terraces. This means that $\nabla \cdot M(r)$ will be unequal to zero at the island edges even if the spin configuration is completely uniform (unless the magnetization points along the edges). Magnetostatics therefore increases the parallel step anisotropy and decreases the perpendicular step anisotropy.

A second effect is more important. At saturation, M_x is a constant and $M_y = 0$. To lowest order, M_x remains constant at nucleation so only the variations of M_y in the y direction contribute to E_{D-D}. The magnetization pattern at nucleation consists of lens-shaped domains centered on those step edges where the local anisotropy axis points in the y direction [23]. At the smallest coverages when the islands are very small, $M_y = M_y(x, y)$ is a function of both x and y so a finite magnetostatic effect is expected. This effect increases as the island size increases initially because more step edge contributes to nucleation. But for large enough island size, the magnetization pattern at nucleation is nearly one dimensional with $M_y = M_y(y)$ for perpendicular step anisotropy and $M_y = M_y(x)$ for parallel step anisotropy. The effect of magnetostatics thus increases in the former case and decreases in the latter case as the islands grow larger. This is the trend seen in Fig. 6.

IV. COMPARISON TO EXPERIMENT

A direct comparison between experiment and the island model results of Fig. 6 is not really justified because, for θ just less than one, the model morphology consists of large disconnected islands separated by long narrow troughs. In reality, island coalescence occurs at these coverages and the morphology is better approximated by a collection of small pits. The pit model of Fig. 1(d) is an idealization of this morphology. We performed simulations for this model also using the Hamiltonian Eq. (1). Figure 9 compares the computed coercive field for the island model (dashed line) and the pit model (light solid line) for the case when the step anisotropy is parallel to the steps. Notice that the coercivity at $\Theta = t + \theta$ for the

island model is similar to the coercivity at $\Theta = t - \theta$ for the pit model. This is because the magnetic reversal is almost the same for islands and depressions of the same size. Small differences occur because the magnetic domain wall energy is not exactly the same in the two cases.

Of course, neither the island model nor the pit model is correct when the coverage is exactly (or very near) t complete layers. A better model would exhibit both small islands and small pits. Based on the foregoing, we would expect the coercivity to be determined by the pits or islands with the longest sides. On the other hand, no large pits form during growth and islands with long sides coalesce to form pits with relatively small step lengths. For this reason, the coercivity never becomes very small. The bold curve in Fig. 9 "synthesizes" this behavior from our island and pit results by removing the unphysical jumps at layer completion and otherwise tracking whichever of the models has the *larger* coercivity.

The single step model explains almost all of the structure that appears in our synthetic $H_C(\Theta)$ curve. When Θ is small, the scale of the oscillations dominates the variations in the mean value of H_C. In the isolated step model, this is the large $\mathcal{K}$ limit when $H_C = H_S$ and is nearly independent of $\mathcal{K}$ but varies with $\mathcal{W}$. Conversely, when Θ is large ($\mathcal{K}$ small), the scale of the oscillations is comparable to the change in the mean value of H_C, which is increasing. This is the small $\mathcal{K}$ limit of the isolated step model where $H_C = H_N$. H_C increases as $\mathcal{K}$ decreases and varies with $\mathcal{W}$ on a comparable scale.

We now are in a position to compare with experiment. Our lower coverage results ($0 \leq \Theta \leq 2$) are relevant to the results of Buckley *et al.* for the Cu/Co/Cu(001) system [13]. There, the observed coercivity decreases very rapidly for submonolayer deposition of copper and then shows a local maximum near $\theta = 1$. In some cases, additional oscillations in H_C were detected. Copper is non-magnetic but our results are still germane because the copper islands break the translational invariance of the surface. The Néel model [7] then predicts that a two-fold anisotropy will be induced for those cobalt atoms that lie just beneath the copper step edges.

For $\Theta \geq 2$, we compare our results with the measurements of Weber *et al.* [12] who

deposited Co on a surface slightly *vicinal* to Cu(001). The presence of steps produces split loop hysteresis curves whose origin we have discussed elsewhere [16]. Here, we focus on the thickness dependence of the *width* of the shifted loop which, as the authors note, corresponds to the coercive field. The basic observation is that H_C exhibits small amplitude, sub-monolayer oscillations superposed on a monotonic rise with increasing coverage. This is in qualitative agreement with the bold curve in Fig. 9.

The authors of Ref. [12] attributed the existence of H_C oscillations to periodic oscillations in the surface morphology as we do. However, owing to the uniaxial anisotropy induced by the steps, they supposed that the presence of *rectangular* islands was the key to the effect. Our results show that oscillations arise even with square islands. Indeed, the isolated step model shows that it is only necessary that there be a periodic change in the length of the steps in one direction.

V. SUMMARY

We have used several classical spin models to study zero temperature hysteresis in ultra-thin films with planar magnetization and surface roughness characteristic of the epitaxial growth process. To lend insight into the complicated situation of many steps, we first discussed a simplified model of a smooth surface with a single finite-length step. The magnetic interactions were taken to be a four-fold anisotropy at all sites, a two-fold anisotropy at step edge sites, and the Zeeman interaction with an external magnetic field. The hysteresis loops that occur were presented in the form of a phase diagram with axes labeled by (scaled) step anisotropy and step length.

We then considered a periodic island and periodic pit model that allowed for one layer of incomplete coverage. Magnetostatic interactions were added at this stage. The characteristic hysteresis fields H_N, H_S, and H_T were found to vary as a function of both film thickness and partial coverage of the surface layer in an explicable manner. As a result, the coercivity exhibited monolayer-scale oscillations on a background that varies non-monotonically with

thickness. These results are all in qualitative agreement with recent experiments for the planar Co/Cu(001) system.

VI. ACKNOWLEDGMENTS

R. A. H. acknowledges support from National Science Foundation Grant No. DMR-9531115 and hospitality from the Department of Physics and Astronomy of the University of Georgia where some of this work was completed. M. D. S. acknowledges useful conversations with R. D. McMichael.

* permanent address: Department of Physics, DePaul University, Chicago IL, 60614

REFERENCES

[1] *Ultrathin Magnetic Structures I*, edited by J.A.C. Bland and B. Heinrich (Springer-Verlag, Berlin, 1994) and *Ultrathin Magnetic Structures II*, edited by B. Heinrich and J. A. C. Bland (Springer-Verlag, Berlin, 1994).

[2] U. Gradmann, in *Handbook of Magnetic Materials*, Volume 7, edited by K.H.J. Buschow (Elsevier, 1993), Chapter 1.

[3] S. D. Bader and J. L. Erskine, in Ref. [1].

[4] P. Bruno, G. Bayreuther, P. Beauvillain, C. Chappert, G. Lugert, D. Renard, J. P. Renard, and J. Seiden, J. Appl. Phys. **68**, 5759 (1990).

[5] S. T. Purcell, M. T. Johnson, N. W. E. McGee, J. J. de Vries, W. B. Zeper, and W. Hoving, J. Appl. Phys. **73**, 1360 (1993); T. Kingetsu, Jpn. J. Appl. Phys. **33**, 1890 (1994).

[6] N. W. E. McGee, M. T. Johnson, J. J. de Vries, and J. aan de Stegge, J. Appl. Phys. **73**, 3418 (1993); T. Kingetsu, Jpn. J. Appl. Phys. Part 2 **33**, L1406 (1994).

[7] L. Néel, J. Phys. Radium **15**, 225 (1954).

[8] M. Albrecht, T. Furubayashi, M. Przybylski, J. Korcki, and U. Gradmann, J. Mag. Mag. Mat. **113**, 207 (1992).

[9] A. S. Arrott, J. Appl. Phys. **69**, 5212 (1991); A. S. Arrott and B. Heinrich, J. Magn. Magn. Mater. **93**, 571 (1991).

[10] A.S. Arrott, T.L. Templeton, and Y. Yoshida, IEEE Trans. Mag. **29**, 2622 (1993); A.S. Arrott, in *Nanomagnetism*, edited by A. Hernando (Kluwer, Amsterdam, 1993), pp. 73-85.

[11] M. Kolesik, M.A. Novotny, and P.A. Rikvold, Phys. Rev. B **56**, 11791 (1997).

[12] W. Weber, C. H. Back, A. Bischof, Ch. Wursch, and R. Allenspach, Phys Rev. Lett. **76**, 1940 (1996).

[13] M. E. Buckley, F. O. Schumann, and J. A. C. Bland, Phys. Rev. B **52**, 6596 (1995); M. E. Buckley, F. O. Schumann, and J. A. C. Bland, J. Phys. Cond. Matt. **8**, L147 (1996).

[14] A. Moschel, R. A. Hyman, A. Zangwill, and M. D. Stiles, Phys. Rev. Lett. **77**, 3653 (1996).

[15] R. A. Hyman, M. D. Stiles, L.-H. Tang, and A. Zangwill, J. Appl. Phys. **81**, 3911 (1997).

[16] R. A. Hyman, A. Zangwill, M. D. Stiles, Phys. Rev. B **58**, 9276 (1998).

[17] The fields here called H_S and H_T were called H_L and $H_\perp$ in Ref. [14] and Ref. [15]. The notation in this paper is the same as Ref. [16].

[18] E. C. Stoner and E. P. Wohlfarth, Phil. Trans. Roy. Soc. A**240**, 74 (1948).

[19] The phases labeled III and IV in Ref. [16] should now be called IIIc and IVc.

[20] S. Clarke and D.D. Vvedensky, J. Appl. Phys. **63**, 2272 (1988).

[21] We have generalized a fast Fourier transform (FFT) technique used for flat films [see, *e.g.* by M. Mansuripur, *The Physical Principles of Magneto-optical Recording* (Cambridge University Press, Cambridge, 1995), Section 13.2] to the case of rough films. By construction, the magnetization is uniform within each spin block. The magnetostatic energy contains an intra-block term and an inter-block term. The intra-block energy accounts for the shape anisotropy of the block. This part of the magnetostatic energy is functionally identical to a bulk crystalline anisotropy that favors in-plane spins. Surface roughness is easily incorporated in this term because it is local and explicitly linear in the thickness. A 2-d FFT magnetostatic routine is used to calculate the inter-block magnetostatic energy. The routine has been derived for uniformly flat films. However, surface roughness can still be incorporated. To lowest order in the thickness, the inter-

block energy is dependent only on the magnetic moments of the blocks. Therefore, surface roughness is included by performing the FFT on an effective flat film in which the magnetization magnitude is adjusted so that the block magnetic moments of the two films are identical. The magnetization in the effective film is $\mathbf{M}_i = t_i M_S \hat{\mathbf{S}}_i$ per site, chosen so that the block magnetic moments of the flat and rough films are identical.

[22] B. Heinrich and J. F. Cochran, Adv. Phys. **42**, 523 (1993). These are the values used in Refs. [14,15]. The size of the four-fold anisotropy was misstated there as $K_4 \sim 1 \times 10^{-2}\mathrm{mJ/m}^2$.

[23] The magnetization pattern at nucleation discussed here is unstable if a jump in magnetization accompanies nucleation. But this pattern is still used to determine the energy barrier to nucleation. See Ref. [16] for more details.

FIGURES

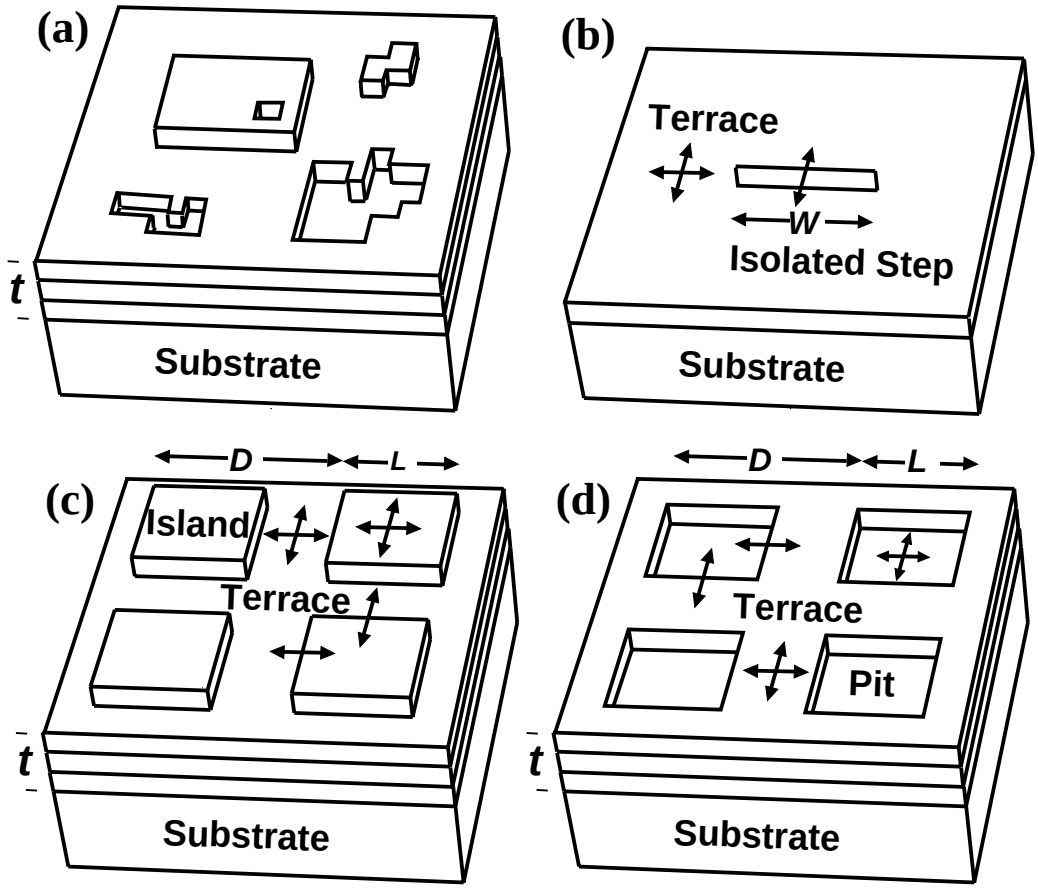

FIG. 1. Schematic view of (a) a "real" ultrathin film; (b) a flat film with a single step; (c) a period island morphology; and (d) a periodic pit morphology. Arrows indicate the easy axes of the in-plane anisotropy.

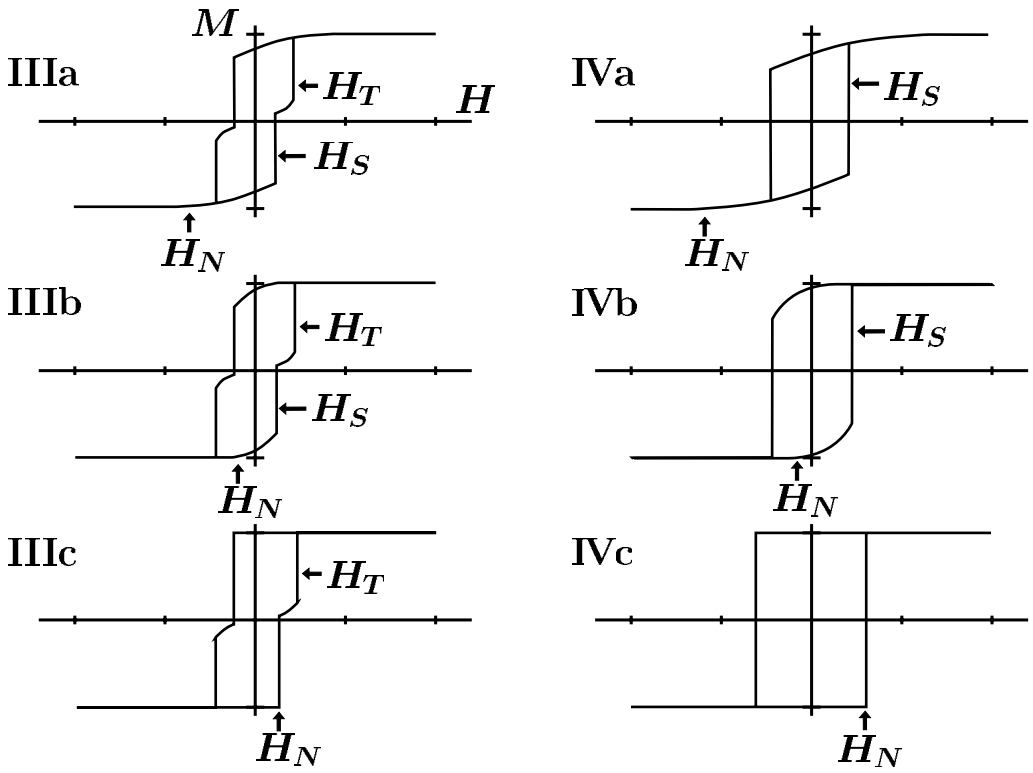

FIG. 2. Hysteresis loops for the isolated step model. The characteristic fields H_N, H_S, and H_T are discussed in the text. The Roman numeral labels correspond to different parts of the phase diagram of Figure 3.

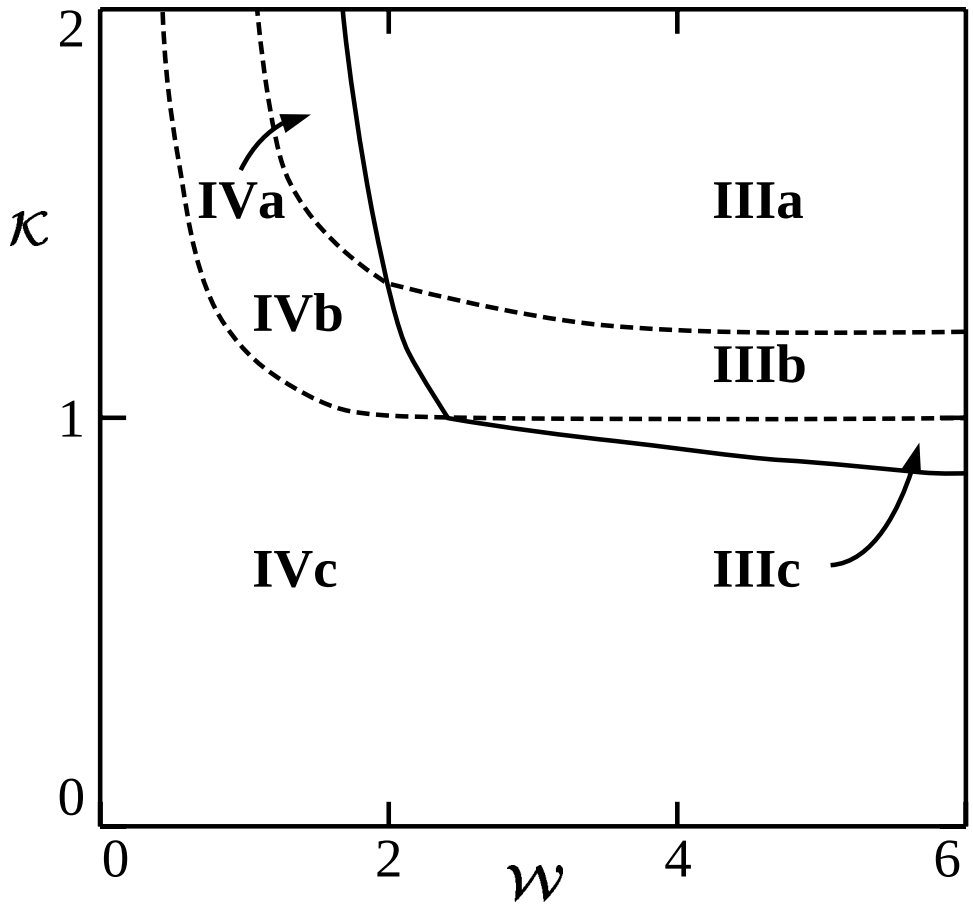

FIG. 3. Loop structure phase diagram for the isolated step model. $\mathcal{K}$ is the scaled step anisotropy and $\mathcal{W}$ is the scaled step width.

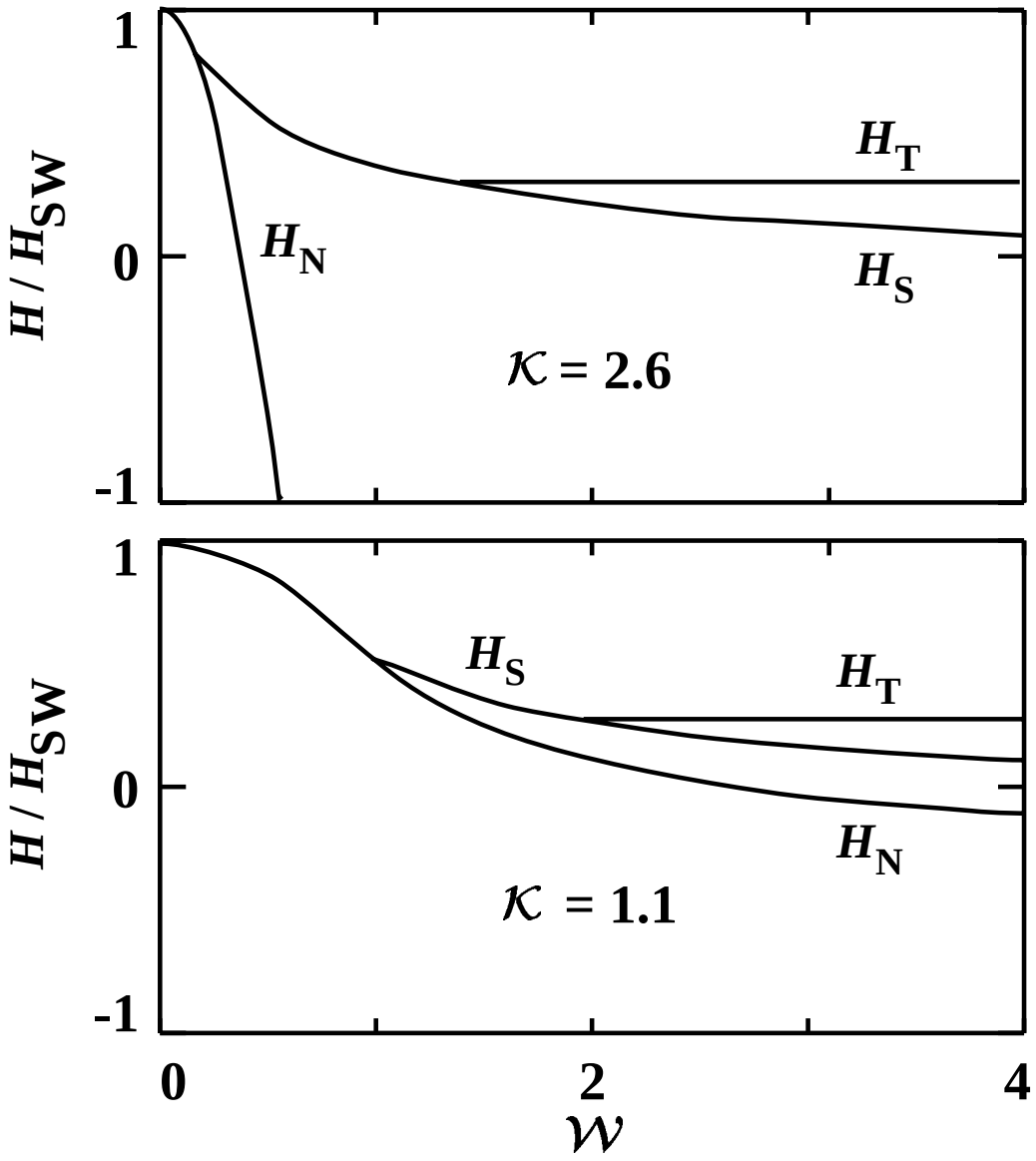

FIG. 4. Characteristic fields as a function of $\mathcal{W}$ for fixed $\mathcal{K}$.

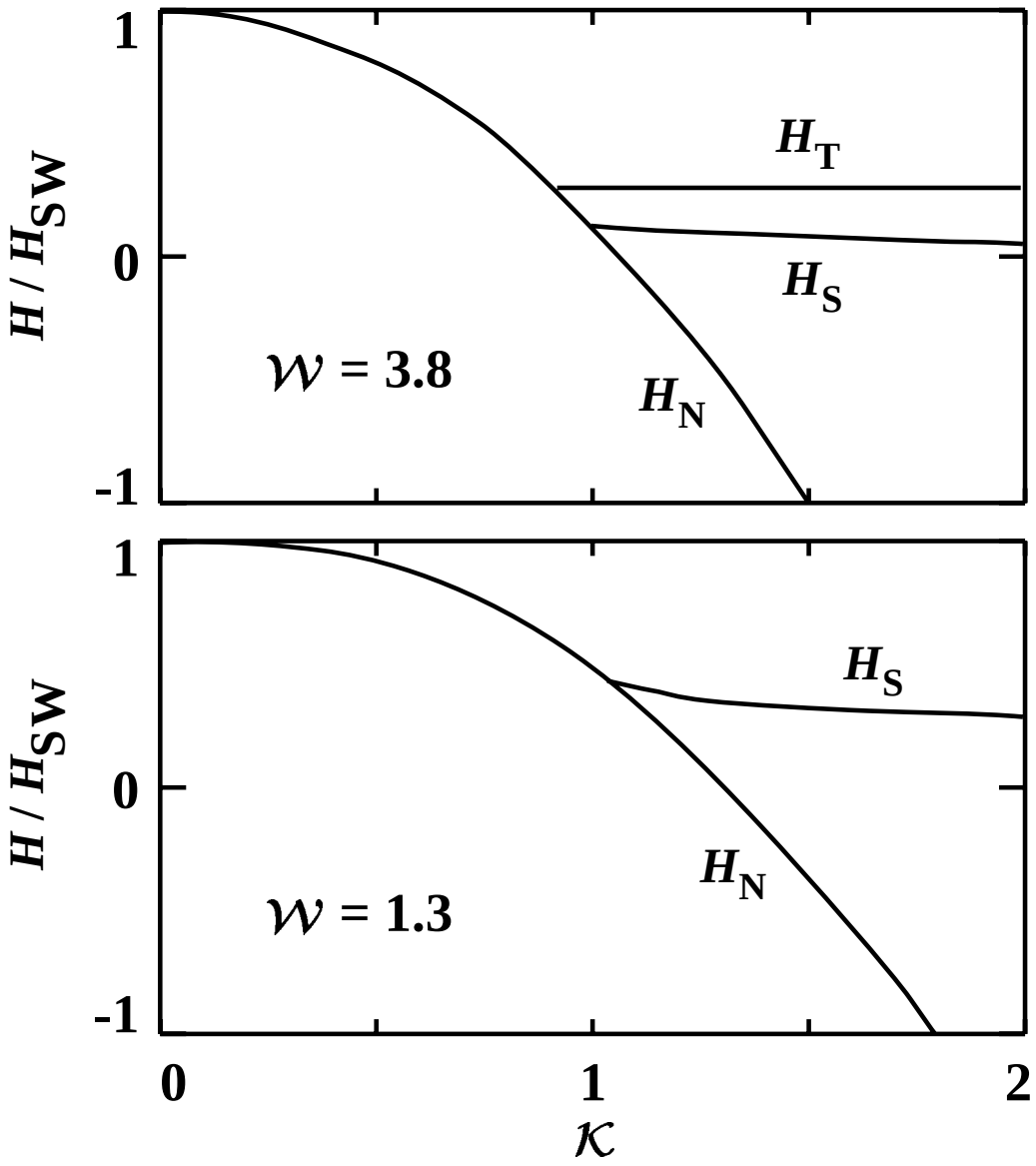

FIG. 5. Characteristic fields as a function of $\mathcal{K}$ for fixed $\mathcal{W}$.

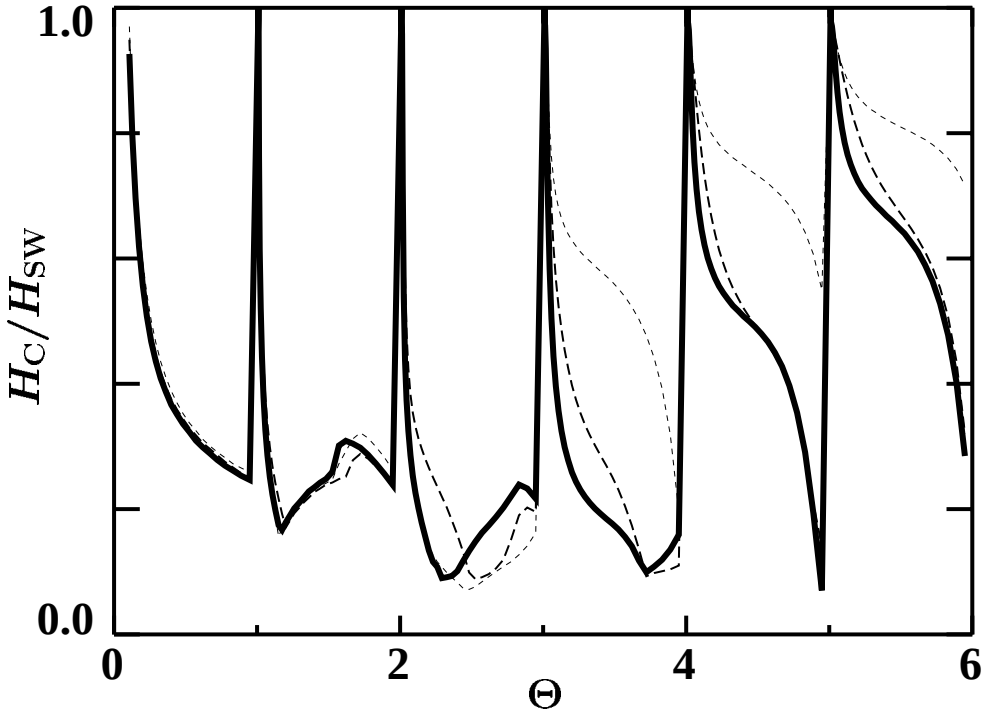

FIG. 6. Scaled coercive field as a function of coverage for the island model. The solid curves give the results without magnetostatics. The heavy dashed curve and light dashed curve give the results with magnetostatics for the cases of step anisotropy parallel and perpendicular to the steps respectively.

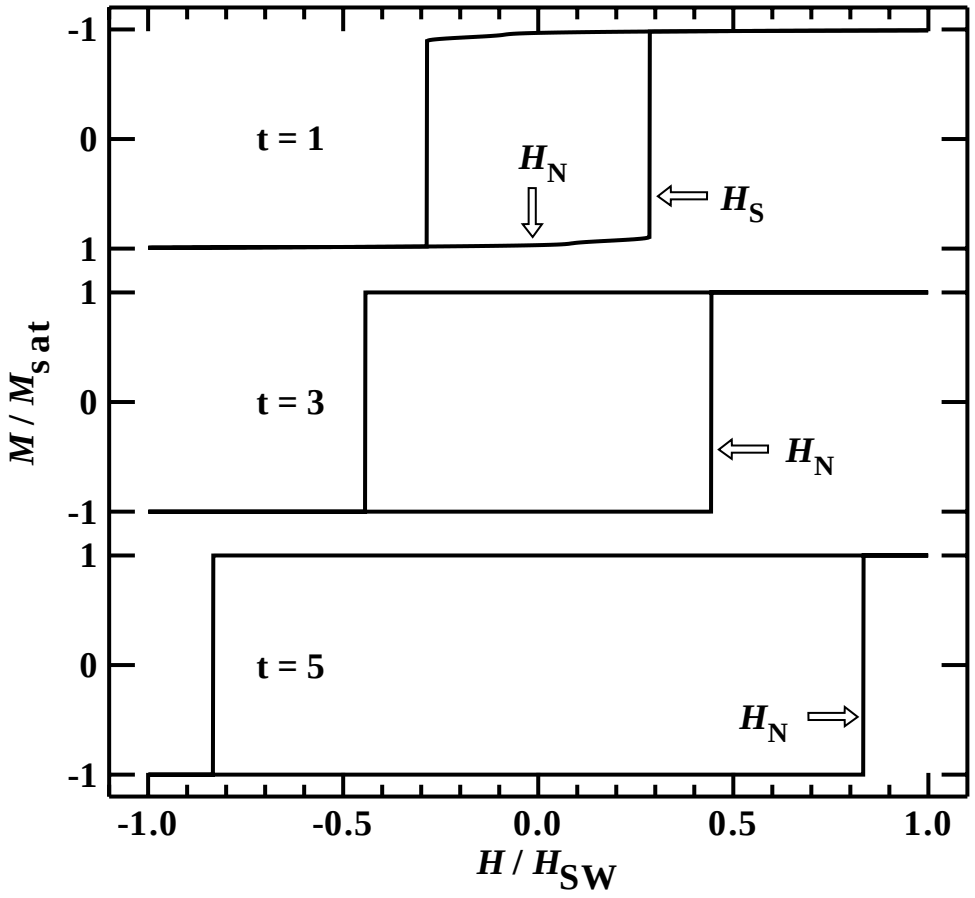

FIG. 7. Hysteresis loops for the island model for $\theta = 0.06$ and $t = 1, 3, 5$.

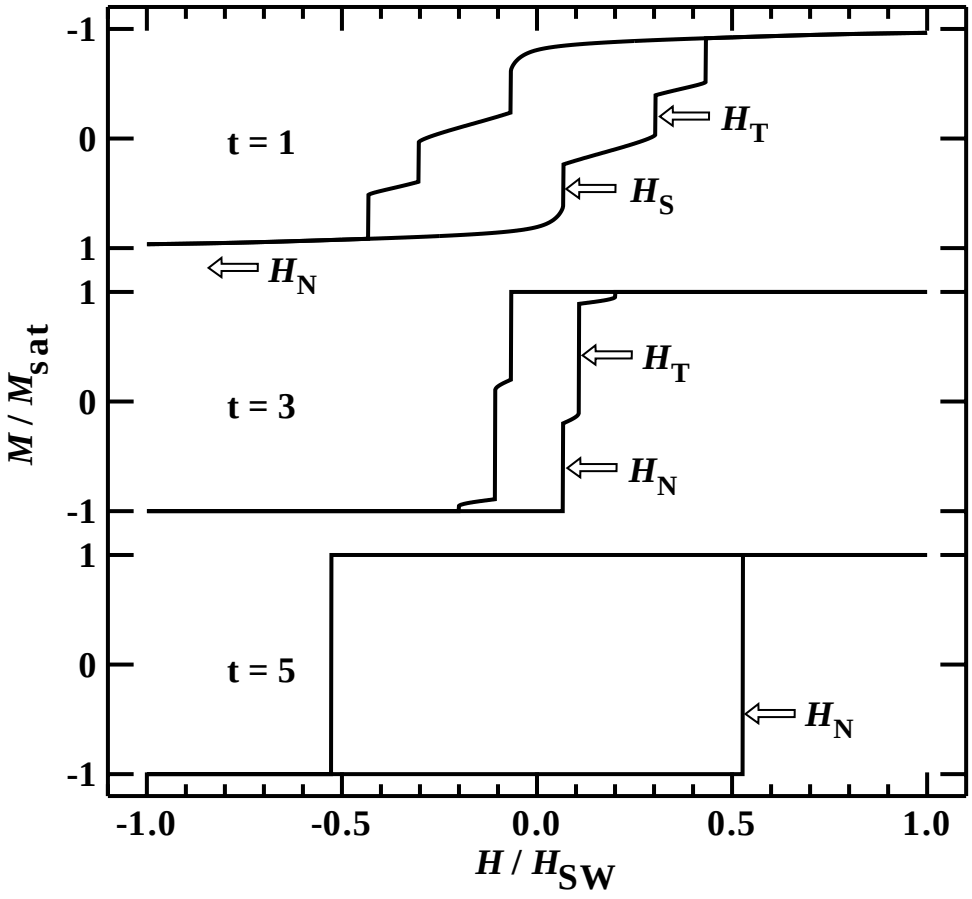

FIG. 8. Hysteresis loops for the island model for $\theta = 0.76$ and $t = 1, 3, 5$.

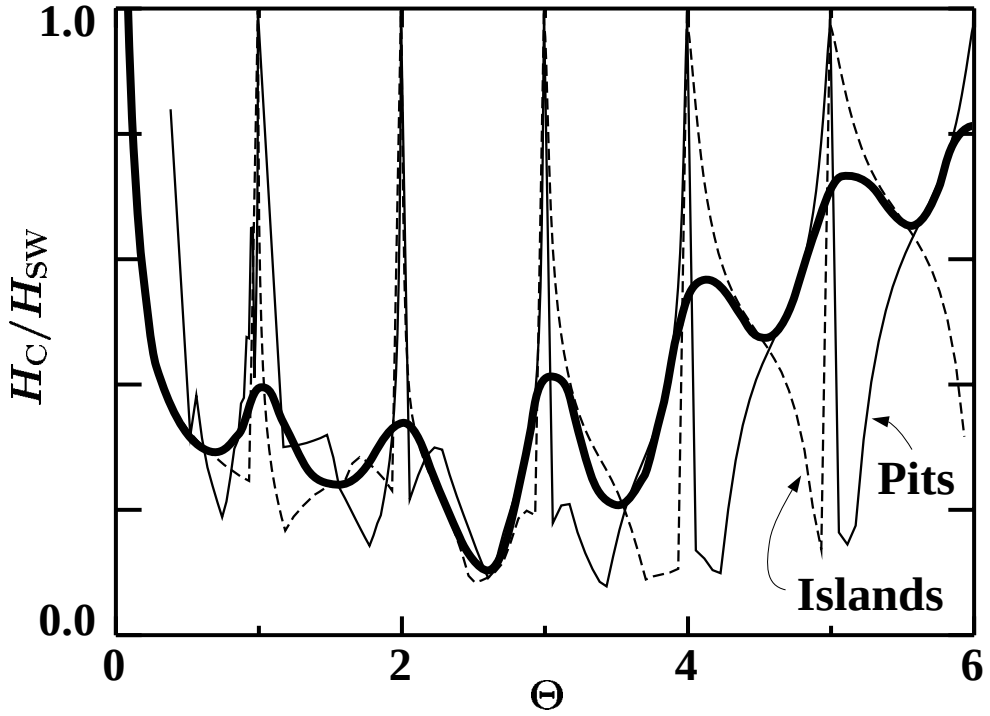

FIG. 9. Scaled coercive field as a function of coverage. The light solid line is the island model. The dashed line is the pit model. The bold solid line synthesizes these two into a curve more suitable for comparison with experiment.